Photogating carbon nanotube transistors

Matthew S. Marcus,[a] J. M. Simmons,[b] and O. M. Castellini[c]
Department of Physics, University of Wisconsin-Madison, 1150 University Avenue, Madison, Wisconsin 53706

R. J. Hamers
Department of Chemistry, University of Wisconsin-Madison, 1101 University Avenue, Madison, Wisconsin 53706

M. A. Eriksson
Department of Physics, University of Wisconsin-Madison, 1150 University Avenue, Madison, Wisconsin 53706

(Received 22 May 2006; accepted 13 July 2006; published online 18 October 2006)

Optoelectronic measurements of carbon nanotube transistors have shown a wide variety of sensitivites to the incident light. Direct photocurrent processes compete with a number of extrinsic mechanisms. Here we show that visible light absorption in the silicon substrate generates a photovoltage that can electrically gate the nanotube device. The photocurrent induced by the changing gate voltage can be significantly larger than that due to direct electron-hole pair generation in the nanotube. The dominance of photogating in these devices is confirmed by the power and position dependence of the resulting photocurrent. The power dependence is strongly nonlinear and photocurrents are measured through the device even when the laser illuminates up to 1 mm from the nanotube. © *2006 American Institute of Physics*. [DOI: 10.1063/1.2357413]

I. INTRODUCTION

Since their discovery, carbon nanotubes have shown great promise for a wide variety of applications including nanoelectromechanical systems[1,2] and chemical and biological sensing.[3,4] The observation of photoconductivity in carbon nanotubes has opened a number of avenues of research in both characterization and photonic applications of nanotubes.[5–7] Photocurrents have been used to characterize the electronic structure of nanotubes, such as the energies of van Hove singularities,[7–9] as well as to image the Schottky barriers between a semiconducting nanotube and the metal contacts,[10] and to build photodetectors using suspended nanotubes.[11] Recently, theory and experiments have shown that the direct photogeneration of carriers is unable to explain the full photophysics of carbon nanotubes and that excitonic[12–14] and environmental (both substrate and gaseous) (Ref. 15) interactions must also be considered. An interesting feature of illuminating nanotube devices on a silicon/silicon dioxide substrate is that the silicon can also absorb light, leading to a voltage at the Si/SiO_2 interface. Such photovoltages can, in many cases, be the dominant component of the induced photocurrent in nanotube devices. Understanding the interaction between the incident light, the back gate, and the nanotube (photo)transistor is important both for potential applications of such devices and for enabling the fundamental understanding of the direct nanotube-light interaction in nanotube transistors.

We show that photovoltages in the silicon gate of carbon nanotube transistors have a significant impact on the measured photocurrent. The measured photocurrent is independent of laser polarization, indicating that direct electron-hole pair generation in the nanotube is negligible. We show that modulating the incident light effectively adds a small ac gate voltage, revealing the derivative of the source-drain current I_{SD} in the photocurrent. Comparing the numerical derivative of the I_{SD} versus gate voltage curve taken without the light to the measured photocurrent as a function of gate voltage, we are able to extract the induced photovoltage which is typically on the order of -10 to -100 mV. Consistent with the photogating effect, the power and position dependence of the measured photocurrent is extremely nonlinear. Indeed, photocurrents persist even when the laser illuminates up to 1 mm away from the nanotube position. The experiments are consistent with a theoretical analysis of the photogating mechanism. These measurements suggest that photovoltages produced in transistor gates may provide the basis for unusual types of photodetectors: devices in which the light absorbed by the gate produces a modulation in a transistor response, as opposed to the direct collection of photogenerated carriers in more conventional photodetectors.

II. EXPERIMENTAL

The carbon nanotubes in the devices studied here are grown by chemical vapor deposition (CVD). Islands of nanotube catalyst are defined using electron-beam lithography,[16] and the nanotubes are grown at 900 °C using a feedstock of methane [400 SCCM (standard cubic centimeter per minute)] with a coflow of hydrogen (20 SCCM).[17–20] The ends of the nanotube are buried under Ti/Au using electron-beam lithography in order to define the source-drain contacts. The nanotube channel and source-drain leads rest on

[a]Present address: Honeywell Laboratories/ACS, 12001 State Highway 55, Plymouth, MN 55441.
[b]Electronic mail: jmsimmons@wisc.edu
[c]Present address: Museum of Science and Industry, 57th Street and Lake Shore Drive, Chicago, IL 60637.

 © 2006 American Institute of Physics

Downloaded 18 Oct 2006 to 129.6.121.139. Redistribution subject to AIP license or copyright, see http://jap.aip.org/jap/copyright.jsp

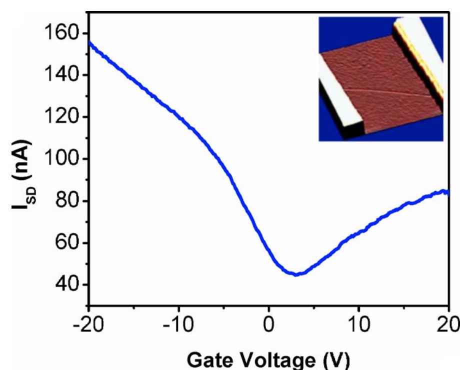

FIG. 1. (Color online) Source-drain current (I_{SD}) as a function of back gate voltage. The conduction through the nanotube increases at large values of both negative and positive gate voltages. Inset: Atomic force microscopy (AFM) image of an ~5 μm long single wall carbon nanotube transistor device.

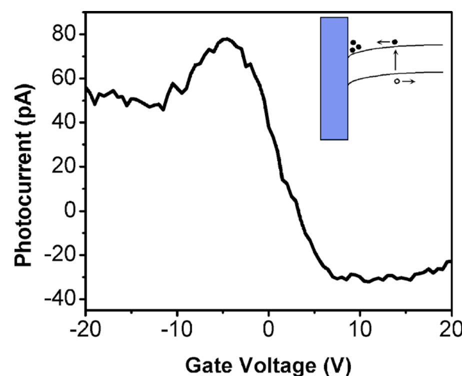

FIG. 2. (Color online) Photocurrent measured through the nanotube channel as a function of gate voltage. The photocurrent switches sign near $V_g=0$. Inset: Schematic of the energy bands with initial band bending at the Si/SiO_2 interface.

top of a 500 nm thick SiO_2 layer that acts as a gate dielectric where the back gate is a heavily doped (nominally $\sim 10^{18}$ cm^{-3}) *p*-Si substrate. Nanotube transistors have been fabricated with both short (~5 μm) and long (~500 μm) channels. Fig. 1 is a plot of the source-drain current (I_{SD}) in a short channel device as a function of gate voltage under a fixed source-drain voltage (V_{SD}=250 mV). The conductance of the nanotube shown is dependent on the gate voltage, and it shows increased conductance at both positive and negative gate voltages. The gate dependence could indicate the presence of a semiconducting nanotube or may indicate effects of two nanotubes in parallel, small metallic gap openings,[21] or resonant electron scattering.[22,23] Regardless of the origin of the gate dependence, all nanotubes that have a gate dependence can respond to photovoltages induced in the gate.

Nanotube devices are illuminated with a P_o=4 mW HeNe laser that has a photon energy (E_γ=1.96 eV) which is larger than both the band gap of our nanotubes[24] as well as the band gap of the Si gate ($E_{G,\mathrm{Si}}$=1.12 eV). For short channel devices the laser always illuminates the entire nanotube device, including the bulk of the nanotube and the metal-nanotube interface. The laser is modulated using an optical chopper and all photocurrents are measured with a lock-in amplifier referenced to the chopping frequency. When the signal is modulated with a chopper, the photovoltage is a step function at the on or off transition, producing a capacitive spike in the current. Once the photovoltage has reached a steady state and is not changing with respect to time, the capacitive current is zero. Slow modulation frequencies (10–100 Hz) are used in order to minimize the effects of capacitive coupling between the source-drain contacts and the gate during the turn on and turn off transitions.[7]

Photocurrents may arise from several sources. These include direct processes, such as electron-hole pairs generated in the nanotube, or indirect processes such as photodesorption[25,26] or photogating. The photocurrent for a nanotube transistor as a function of gate voltage is shown in Fig. 2 and, intriguingly, changes sign as a function of gate voltage. Also, the photocurrent shows no dependence on the polarization of the laser with respect to the nanotube axis.[7,10] The change in sign of the photocurrent in Fig. 2 and the absence of polarization dependence indicates that direct processes are not the source of the observed photocurrent. Direct photocurrent in a biased nanotube would have the same sign for all applied gate voltages because the electric field provided by the bias voltage would sweep all the photogenerated carriers in the same direction, independent of the gate voltage. The photodesorption of oxygen from the metal-nanotube contacts also cannot account for the observed photocurrent. The removal of oxygen from the nanotube and/or contacts, thereby affecting the metal-nanotube Schottky barrier, would lead to decreases in the *p*-channel conductivity (negative gate voltages) and increases in the *n*-channel conductivity (positive gate voltages).[26] The data in Fig. 2 show an increase in *p*-channel conductivity and a decrease in the *n*-channel conductivity, the opposite of what is expected for a photodesorption process. Photogating, as we show below, can explain both the increased *p* channel and decreased *n*-channel conductivity as well as the observed sign change.

III. PHOTOGATING MECHANISM

Photogating occurs when photoexcited charge in the silicon gate causes a change in potential (δV_{PV}) at the Si/SiO_2 interface. In order for photogating to occur, there needs to be a slope in the Si energy bands at the Si/SiO_2 interface. Bending in the Si energy bands provides an electric field that separates the electron-hole pairs produced by the laser and a potential well to trap either electrons or holes.[27,28] Band bending is often present due to charge in the oxide (mobile ions, fixed charge, and interface states) which induces a depletion region near the Si/SiO_2 interface. In addition to the presence of band bending, to produce a significant photovoltage the potential well must be deep enough to act as a trap at the measurement temperature (~25 meV).

In order to determine if there is band bending at the Si/SiO_2 interface, capacitance-voltage (*CV*) characteristics of a metal-oxide-semiconductor capacitor (MOSC) are measured.[29,30] The MOSC is fabricated on an oxidized Si wafer from the same batch as the nanotube samples studied. Fits to the experimental *CV* data (not shown) indicate that the bulk doping concentration is $N_a \approx 1.2 \times 10^{18}$ cm^{-3} and that there is an offset voltage ΔV_o=−28 V. The nonzero offset voltage indicates the presence of initial band bending due

Downloaded 18 Oct 2006 to 129.6.121.139. Redistribution subject to AIP license or copyright, see http://jap.aip.org/jap/copyright.jsp

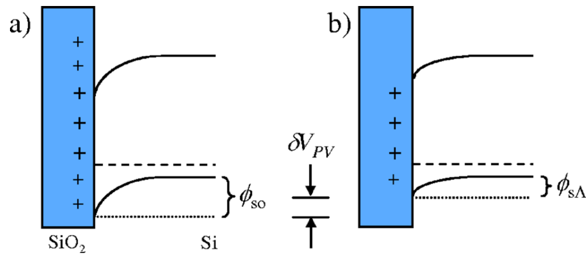

FIG. 3. (Color online) Schematic band diagrams showing band bending ϕ_s in the silicon substrate for the as fabricated device (a) and under laser illumination (b). For typical oxide charge densities, the initial band bending ϕ_{so} is ~100–200 mV. Under illumination, the positive oxide charge is partially screened by photogenerated electrons that become trapped at the interface, reducing the surface potential from $\phi_{so} \rightarrow \phi_{s\Lambda}$. The resulting photovoltage δV_{PV} is given by Eq. (3).

to oxide charge. If the offset voltage were zero there would be no curvature in the Si energy bands and therefore no photogating effect. The oxide charge density can be estimated using $N_{ox} \approx -C_{ox}\Delta V_o/e \approx 1.2\times 10^{12}$ cm^{-2}, where C_{ox} is the capacitance per area of the oxide and e is the magnitude of the electron charge. The positive oxide charge induces an equal negative charge in the silicon substrate ($Q_s = -N_{ox} \approx -1.2\times 10^{12}$ cm^{-2}), such that the energy bands in the silicon are bent downwards, establishing a trap for photoexcited electrons.

In order to produce a photovoltage, the magnitude of the potential created as a result of oxide charge must be significant enough to provide an electric field that can redistribute the electron-hole pairs generated by the laser. The charge in the silicon is a function of the surface potential [band bending, see Fig. 3(a)] ϕ_s and is given by the expression[27]

$$Q_s = -\sqrt{2k_BT\varepsilon_{Si}n_i}F(U_s,U_b,\Delta n), \quad (1)$$

where

$$F(U_s,U_b,\Delta n) = [e^{U_b}(e^{-U_s}+U_s-1) + e^{-U_b}(e^{U_s}-U_s-1) + \Lambda e^{U_b}(e^{U_s}+e^{-U_s}-2\ ]^{1/2} \quad (2)$$

is the normalized interfacial electric field, assuming that the depletion width is smaller than the diffusion length and that recombination currents can be ignored. In the previous equations k_B is Boltzmann's constant, T is temperature, ε_{Si} is the dielectric constant of Si, n_i is the intrinsic number of carriers, U_s and U_b are the normalized surface and bulk potential $U_s = q\phi_s/k_BT$, $U_b = \ln(N_a/n_i)$, and Λ is the ratio of photoexcited carriers to the equilibrium number of majority carriers $\Lambda = \Delta p/p_o = \Delta n/p_o$, also referred to as the injection ratio. Due to the complexity of Eq. (2), the magnitude of the potential is most easily found graphically or numerically. First, in the absence of light, $F(U_s,U_b,\Delta n)$ becomes a function only of the surface potential ϕ_s. Using the value of Q_s determined above, $F(U_s,U_b,\Delta n=0) \equiv F_o$ is computed using Eq. (1). The value of F_o is shown as the dotted line in the inset of Fig. 4. Next, using Eq. (2), F is plotted as a function of ϕ_s and the intersection of the curve with the dotted line sets the initial amount of potential ϕ_{so} due to the oxide charge. For the MOSC, the potential ϕ_{so}, shown schematically in Fig. 3(a), is measured to be ~120 mV which is larger than the thermal

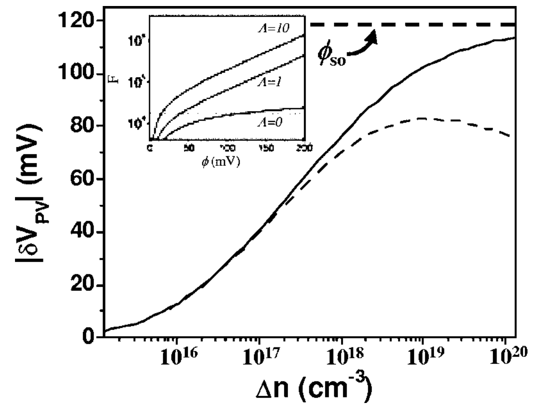

FIG. 4. Calculated magnitude of photovoltage as a function of the number of photoexcited carriers, assuming a bulk doping density of $N_a \approx 1.2\times 10^{18}$ cm^{-3} and an initial surface potential of $\phi_{so} \sim 120$ mV. The solid line includes only the effect of the initial band bending. The dotted line includes the effect of the Dember voltage (see appendix). Inset: Calculated normalized electric field at the Si/SiO_2 interface as a function of the surface potential and injection ratio. The dotted line indicates the value of the field F_o as determined from the initial charge in the silicon Q_s.

carrier energies, enabling photogenerated electrons to be trapped at the Si/SiO_2 interface.

Photoexcited electrons and holes in the silicon are separated by the interfacial electric field. This charge redistribution changes the potential in the silicon from ϕ_{so} to a different value $\phi_{s\Lambda}$ [Fig. 3(b)]. The difference between the two potentials is the measured photovoltage,

$$\delta V_{PV} = \phi_{s\Lambda} - \phi_{so}. \quad (3)$$

So long as the laser does not affect the amount of oxide charge, the total charge in the silicon remains constant and, according to Eq. (1), the value of F must stay fixed at F_o. When illumination causes Λ to become nonzero, U_s, and therefore ϕ_s, must change to keep $F=F_o$. The inset of Fig. 4 shows several different F vs ϕ_s curves as the injection ratio Λ is varied. The potential under illumination $\phi_{s\Lambda}$ is the intersection point between the curve for a given Λ and the initial interfacial field F_o. For low values of the injection ratio, there are few photogenerated carriers to fill the potential well at the Si/SiO_2 interface and $\phi_{s\Lambda} \approx \phi_{so}$. As the injection ratio is increased, there are more carriers to fill the well and the bands become less curved, reaching flat band conditions for high values of Λ. Thus, as the injection ratio increases, the measured photovoltage will change from 0 to $-\phi_{so}$. The magnitude of the resulting photovoltage is plotted as a function of photocarrier density in Fig. 4, using a bulk silicon doping density of $N_a \sim 1.2\times 10^{18}$ cm^{-3} ($\Delta n = \Lambda N_a$) and the measured initial surface potential $\phi_{so} \sim 120$ mV. Once the bands are flat ($\phi_{s\Lambda}=0$), there is no electric field to separate the electrons and holes and the measured photovoltage saturates. This is illustrated in Fig. 4 where the photovoltage asymptotically approaches ϕ_{so} when Λ becomes large and in the inset where the interface potential tends to 0. It is important to note that since different processing conditions can lead to changes in the initial surface potential, photovoltages measured on different samples can have higher or lower values than the maximum presented in Fig. 4.[29] Also, for sufficiently high-injection ratios ($\Delta n \gtrsim p_o$), other pro-

Downloaded 18 Oct 2006 to 129.6.121.139. Redistribution subject to AIP license or copyright, see http://jap.aip.org/jap/copyright.jsp

cesses, such as the Dember voltage[28] presented in the appendix, can become important and could dominate over the photovoltage due to initial band curvature as shown by the dashed curve in Fig. 4. As we show next, we remain in the low-injection limit where these additional effects can be ignored.

In the limit of low-injection conditions, $\Delta n < p_o$, we can estimate the number of excited carriers as[27]

$$\Delta n \approx \frac{I\alpha L_n}{(1+\alpha L_n)(s_1 + D_n/L_n)} \lesssim 10^{17}\ \text{cm}^{-3}, \quad (4)$$

where $\alpha \approx 3000\ \text{cm}^{-1}$ is the absorption coefficient[30] of Si at $\lambda = 633$ nm, $D_n = 7\ \text{cm}^2/\text{s}$ is the minority carrier diffusion coefficient, $L_n = 45\ \mu\text{m}$ is the diffusion length, I is the photon intensity, and s_1 is the surface recombination velocity at the Si/SiO_2 interface. The diffusion coefficient $(D_n = k_B T/q\mu_n)$ and diffusion length $(L_n = \sqrt{D_n \tau_n})$ are calculated using the minority carrier recombination lifetime[31] $\tau_n = 3\times 10^{-6}$ s and the minority carrier drift mobility[30] $\mu_n \sim 270\ \text{cm}^2/\text{V s}$. The photon intensity is given by $I = \xi\eta(1-R)2P_o/eE_\gamma \pi\omega^2$, where η is the quantum efficiency (assumed to be unity), $R = 0.5$ is the measured reflectivity of the Si, and $\omega \sim 20\ \mu\text{m}$ is the estimated laser spot radius. The factor of $\xi = 0.2$ is used to account for the portion of the laser power incident on the underlying silicon that is not absorbed by the metal leads. The surface recombination velocity depends on a variety of factors including interface state density, gate voltage, and the number of photoexcited carriers,[32] and is typically on the order of 100–1000 cm/s. As an order of magnitude estimate, we assume that s_1 is negligible, which is valid as long as $s_1 < D_n/L_n \approx 1500$ cm/s. Due to our approximations for s_1 and η and because Eq. (4) does not account for the diffusion of carriers parallel to the Si/SiO_2 interface, the calculated value is an overestimate of the photoexcited carrier density. This overestimate confirms that we are in the low-injection limit $(\Delta n < N_a \approx 10^{18}\ \text{cm}^{-3})$ for our experimental conditions. Using Δn and Fig. 4, the photovoltage is estimated to be $\delta V_{PV} < -40$ mV. The actual photovoltage measured in the experiment is extracted and is compared to this value later.

IV. DISCUSSION

The photovoltage produced in the silicon gate couples into the nanotube circuit by providing an additional gate voltage for the nanotube channel. When the light is modulated, the effective gate voltage is $V_g = V_{dc} + \delta V_{PV}(t)$, where δV_{PV} is the time dependant photovoltage and V_{dc} is an existing gate voltage applied by a battery. Since the current in the channel is measured with a lock-in amplifier, the measured photocurrent is $I_{PC} = (\partial I_{SD}/\partial V_g)\delta V_{PV}$. Thus, the data shown in Fig. 2 may be understood as a derivative measurement of Fig. 1, and the photocurrent reveals the change in the source-drain current due to the addition of a small negative ac gate voltage to the existing dc gate voltage. From Fig. 1 we see that adding a small negative gate voltage to an existing negative gate voltage causes the source-drain current to increase, yielding a positive derivative and positive photocurrent. At

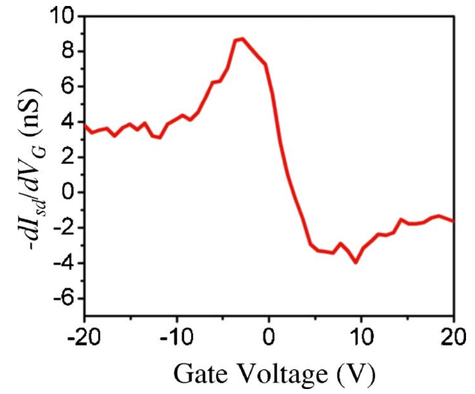

FIG. 5. (Color online) Numerically calculated derivative from the data in Fig. 1. The form of the derivative is extremely similar to the measured photocurrent in Fig. 2 where the *p*-channel conduction is increased and the *n*-channel is suppressed.

positive gate voltages, the effect of adding a small negative gate voltage causes the source-drain current to decrease, yielding a negative photocurrent.

The magnitude of the photogated photocurrent depends on both the nanotube-gate coupling $\partial I_{SD}/\partial V_g$ and the photovoltage δV_{PV} at the Si/SiO_2 interface. The photovoltage can be extracted by dividing the photocurrent signal by the gate derivative $\partial I_{SD}/\partial V_g$, which is calculated numerically from the data in Fig. 1 and is shown in Fig. 5. The photovoltage for this device is $\delta V_{PV} = -15$ mV and is independent of the applied gate voltage. This measured value of photovoltage is similar to the overestimate calculated above, supporting the photogating mechanism.

The power dependence of the photocurrent is another important parameter for establishing the role of photogating. The generation rate of photocarriers is linear with laser power, both in the nanotube and in the silicon. For a direct photocurrent process in the nanotube I_{PC} is expected to be proportional to the generation rate, whereas for photogating $I_{PC} \propto \delta V_{PV}$ which is nonlinear in the number of excited carriers. Using neutral density filters to change the incident laser intensity, the photocurrent as a function of power was measured on a long channel nanotube device[33] and is shown in Fig. 6. Using the nanotube-gate coupling and the measured photocurrent, the induced photovoltage for this device was

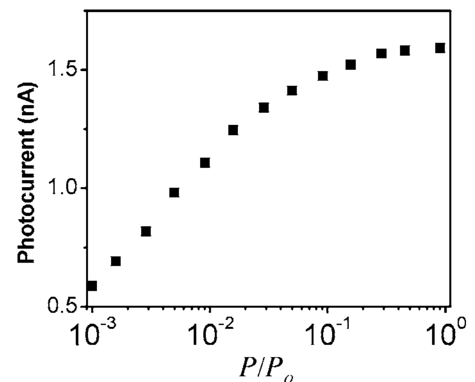

FIG. 6. Measured photocurrent as a function of the incident laser power on a long channel nanotube device. The nonlinearity of the intensity dependence indicates that the photocurrent does not arise from a direct process.

Downloaded 18 Oct 2006 to 129.6.121.139. Redistribution subject to AIP license or copyright, see http://jap.aip.org/jap/copyright.jsp

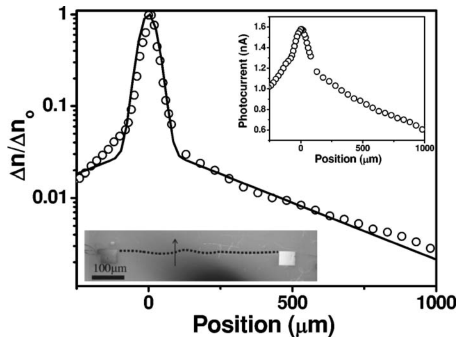

FIG. 7. Ratio of photogenerated electrons in the silicon substrate as a function of position. The circles are the experimentally measured values, extracted by relating the raw photocurrent vs position in the upper inset to the intensity dependence shown in Fig. 6. The line is a fit to Eq. (5) which includes the direct generation of carriers beneath the nanotube as well as the diffusion of carriers when the laser illuminates away from the nanotube. Upper inset: Photocurrent as a function of position perpendicular to the long axis of nanotube. Photocurrent is measured up to 1 mm away from the nanotube. Lower inset: scanning electron microscopy (SEM) image of the ~500 μm nanotube device, where the dotted line indicates the position of the nanotube. The arrow shows the position and direction of the scanned laser.

measured to be $\delta V_{\mathrm{PV}}=-160$ mV. Similar to Fig. 4, the photocurrent changes logarithmically under low injection before saturating at high laser intensities.

It is interesting to note that the photovoltage depends only weakly on where the laser illuminates the sample relative to the nanotube. This fact is illustrated in the upper inset to Fig. 7, which shows the photocurrent as a function of position perpendicular to the long axis of the nanotube at the position indicated by the arrow in the lower inset. The curve is slightly asymmetric about the position of the nanotube due to the proximity of the device to the edge of the silicon chip. The surprising feature of Fig. 7 is that there is an appreciable photocurrent, reduced only by a factor of ~3, even when the laser spot is centered over 1 mm away from the device. Using a laser spot with an ~60 μm Gaussian width, there are virtually no carriers produced near the nanotube at such a large distance from the nanotube. Since the laser is not producing carriers near the nanotube, the carriers must be mobile in the Si. Thus the photocurrent that is induced by the photovoltage arises from laser generated carriers near the nanotube as well as carriers that diffuse towards the nanotube. We can phenomenologically express the number of carriers under the nanotube as

$$\Delta n(x)/\Delta n_o = A e^{-2x^2/\omega^2} + B e^{-|x|/L_n}, \tag{5}$$

where the first term accounts for the direct photogeneration of carriers in the silicon under the nanotube and the second term is from carriers generated at some distance from the nanotube diffusing towards the nanotube. Using Fig. 6 to relate the photocurrent to incident power, and since Δn is proportional to the laser power, we can relate the measured photocurrent to the ratio of $\Delta n(x)/\Delta n_o$, where Δn_o is the number of carriers generated in the silicon at the photocurrent maxima. The solid line in Fig. 7 is a fit to the experimental data using Eq. (5), with the exponential prefactors A and B, the beam waist ω, and the diffusion length L_n as free parameters. The experimental data are well fitted by Eq. (5) using $\omega=58$ μm and $L_n=350$ μm. The extracted value of L_n is an effective diffusion length, as opposed to the bulk diffusion length and can depend greatly on the detailed geometry and injection conditions that are present. These results illustrate that photogating is a long-range interaction. Carriers that are generated in the silicon substrate millimeters away from the nanotube still have a significant effect on the nanotube circuit.

Photogated nanotube devices present an interesting alternative to photodetection on the nanoscale. Such a device would separate the absorption of photons from the detection current, such that each can be independently optimized. The gate material (silicon in this case) would determine the absorption properties of the detector, and could be modified to increase the absorption cross section at the desired wavelengths. The sensitivity of the photogated nanotube detector is determined by the nanotube-gate coupling $\partial I_{SD}/\partial V_g$, which may be custom tailored through device engineering of the Schottky barriers,[34] and geometry, as well as the mode of operation (subthreshold versus on).[35] Nanotubes offer many properties that make them superior channel materials such as high mobilities[36] and large saturation velocities,[37] but there is no reason to expect that photogating of the type studied here should be unique to carbon nanotube channels.

In conclusion we have demonstrated that light absorption in the substrate of carbon nanotube field effect transistors generates an extra photovoltage at the Si/SiO_2 interface. This photovoltage acts as an additional negative gate voltage of the order of 10–100 mV on the nanotube transistor and, depending on the magnitude of the nanotube-gate coupling, produces changes in the source-drain current of up to ~2 nA which is considerably larger than previously reported photocurrents in carbon nanotubes.[7,8] The photovoltage responds nonlinearly to the power in the laser beam, increasing only by a factor of 3 over three orders of magnitude in laser power, and is only weakly dependent on where the carriers are generated with respect to the nanotube. We find that the charge generated in the Si substrate up to 1 mm away from the nanotube still produces a measurable photocurrent. The current due to photogating can, in many cases, be the dominant component of the photocurrent measured through nanotube transistors and must be accounted for in order to determine the intrinsic/direct photocurrent in nanotube devices. Though photogating complicates the analysis of photocurrent measurements, it also offers a different mode of photodetection where the absorption and detection elements are separate. This style of detection would allow for the individual optimization of the photoabsorber and the electronic sensitivity of the transistor channel.

ACKNOWLEDGMENTS

We would like to acknowledge Jennifer Sebby-Strabley for useful discussions. We would also like to acknowledge funding from the NSF CAREER program under Grant No. DMR-0094063, the NSF MRSEC program under Grant No. DMR-0520527, and the NSF NSEC program under Grant No. DMR-0425880.

Downloaded 18 Oct 2006 to 129.6.121.139. Redistribution subject to AIP license or copyright, see http://jap.aip.org/jap/copyright.jsp

APPENDIX: DEMBER VOLTAGE

In addition to a potential forming from the redistribution of photoexcited charge, another voltage that can form in the substrate, the Dember voltage, is particularly relevant for high-injection conditions where $\Delta n \gtrsim p_o$. The Dember voltage is produced when photoexcited electrons and holes diffuse at different rates. The differing diffusion rates lead to a separation of the charge, which in turn generates an electric field in the silicon substrate. Because the electron mobility is higher than the hole mobility in silicon, the sign of the Dember voltage is always positive and will appear in series with the band-induced photovoltage, effectively reducing the total amount of photovoltage measured in the nanotube device. The Dember voltage is expressed as[28]

$$V_d = \frac{k_B T}{e} \frac{b-1}{b+1} \ln\left[1 + \frac{(b+1)\Delta n}{n_o + b p_o}\right], \tag{A1}$$

where b is the ratio of electron to hole mobility $\mu_n/\mu_p \sim 1.8$ and n_o is the equilibrium number of electrons in the silicon. Using the overestimated value of Δn from Eq. (4), the Dember voltage in our devices is $V_d \approx 1$ mV which is much less than the measured photovoltage due to band curvature for the analysis presented here. For larger values of excited carriers, the Dember voltage can become comparable to the photovoltage and should not be ignored. The effect of the Dember voltage is shown in Fig. 4, where the calculated total photovoltage for the case when there is only band curvature (solid line) is compared to when the Dember voltage is included (dotted line), assuming a bulk doping density of $N_a \approx 1.2 \times 10^{18}$ cm^{-3} and initial band bending of $\phi_{so} = -120$ mV. As can be seen, the effect of the Dember voltage is small under low-injection conditions but becomes sizable when the number of injected carriers nears the bulk doping density. It is important to note that both the band curvature and Dember voltages depend on the bulk doping and oxide charge densities and must be recalculated if higher or lower doping concentrations are used.

[1] V. Sazonova, Y. Yaish, H. Üstünel, D. Roundy, T. A. Arias, and P. L. McEuen, Nature (London) **431**, 284 (2004).
[2] A. M. Fennimore, T. D. Yuzvinsky, W.-Q. Han, M. S. Fuhrer, J. Cumings, and A. Zettl, Nature (London) **424**, 408 (2003).
[3] C. S. Lee, S. E. Baker, M. S. Marcus, W. Yang, M. A. Eriksson, and R. J. Hamers, Nano Lett. **4**, 1713 (2004).
[4] A. Star, E. Tu, J. Niemann, J. C. P. Gabriel, C. S. Joiner, and C. Valcke, Proc. Natl. Acad. Sci. U.S.A. **103**, 921 (2006).
[5] A. Fujiwara *et al.*, Jpn. J. Appl. Phys., Part 2 **40**, L1229 (2001).
[6] I. A. Levitsky and W. B. Euler, Appl. Phys. Lett. **83**, 1857 (2003).
[7] M. Freitag, Y. Martin, J. A. Misewich, R. Martel, and Ph. Avouris, Nano Lett. **3**, 1067 (2003).
[8] Y. Ohno, S. Kishimoto, T. Mizutani, T. Okazaki, and H. Shinohara, Appl. Phys. Lett. **84**, 1368 (2004).
[9] A. Mohite, G. Sumanasekera, K. Hirahara, S. Bandow, S. Iijima, and B. Alphenaar, Chem. Phys. Lett. **412**, 190 (2005).
[10] K. Balasubramanian, Y. Fan, M. Burghard, K. Kern, M. Friedrich, U. Wannek, and A. Mews, Appl. Phys. Lett. **84**, 2400 (2004).
[11] H.-C. Yuan, B. Yang, J. M. Simmons, M. S. Marcus, Z. Ma, M. A. Eriksson, and M. G. Lagally, in *Photonic Applications in Nonlinear Optics, Nanophotonics, and Microwave Photonics* (SPIE, Toronto, Canada, 2005), Vol. 5971, p. 597118.
[12] E. J. Mele and C. L. Kane, Solid State Commun. **135**, 527 (2005).
[13] Y. Z. Ma, L. Valkunas, S. M. Bachilo, and G. R. Fleming, J. Phys. Chem. B **109**, 15671 (2005).
[14] C.-X. Sheng, Z. V. Vardeny, A. B. Dalton, and R. H. Baughman, Phys. Rev. B **71**, 125427 (2005).
[15] M. E. Itkis, F. Borondics, A. Yu, and R. C. Haddon, Science **312**, 413 (2006).
[16] J. Kong, H. T. Soh, A. M. Cassell, C. F. Quate, and H. Dai, Nature (London) **395**, 878 (1998).
[17] Carbon nanotubes are grown in a FirstNano CVD system. FirstNano, Inc., 1860 Smithtown Ave., Ronkonkoma, NY 11779.
[18] A. V. Melechko, V. I. Merkulov, T. E. McKnight, M. A. Guillorn, K. L. Klein, D. H. Lowndes, and M. L. Simpson, J. Appl. Phys. **97**, 041301 (2005).
[19] A. Moisala, A. G. Nasibulin, and E. I. Kauppinen, J. Phys.: Condens. Matter **15**, S3011 (2003).
[20] J. M. Simmons, B. M. Nichols, M. S. Marcus, O. M. Castellini, R. J. Hamers, and M. A. Eriksson, Small **2**, 902 (2006).
[21] M. Ouyang, J. L. Huang, C. L. Cheung, and C. M. Lieber, Science **292**, 702 (2001).
[22] M. Bockrath, W. Liang, D. Bozovic, J. H. Hafner, C. M. Lieber, M. Tinkham, and H. Park, Science **291**, 283 (2001).
[23] D. Bozovic, M. Bockrath, J. H. Hafner, C. M. Lieber, H. Park, and M. Tinkham, Phys. Rev. B **67**, 033407 (2003).
[24] Nanotubes with diameters larger than ~0.5 nm have band gaps that are less than the photon energy of our laser.
[25] R. J. Chen, N. R. Franklin, J. Kong, J. Cao, T. W. Tombler, Y. Zhang, and H. Dai, Appl. Phys. Lett. **79**, 2258 (2001).
[26] M. Shim and G. P. Siddons, Appl. Phys. Lett. **83**, 3564 (2003).
[27] D. K. Schroder, Meas. Sci. Technol. **12**, R16 (2001).
[28] L. Kronik and Y. Shapira, Surf. Sci. Rep. **37**, 1 (1999).
[29] D. K. Schroder, *Semiconductor Material and Device Characterization* (Wiley Interscience, New York, 1998).
[30] S. Sze, *Physics of Semiconductor Devices* (Wiley, New York, 1981).
[31] M. S. Tyagi and R. Van Overstraeten, Solid-State Electron. **26**, 577 (1983).
[32] A. G. Aberle, S. Glunz, and W. Warta, J. Appl. Phys. **71**, 4422 (1992).
[33] This device was grown using an iron nitrate catalyst at 900 °C, with 500 SCCM hydrogen, 1000 SCCM methane, and 20 SCCM ethylene.
[34] S. Heinze, J. Tersoff, and Ph. Avouris, Appl. Phys. Lett. **83**, 5038 (2003).
[35] J. Appenzeller, J. Knoch, V. Derycke, R. Martel, S. Wind, and Ph. Avouris, Phys. Rev. Lett. **89**, 126801 (2002).
[36] T. Durkop, S. A. Getty, E. Cobas, and M. S. Fuhrer, Nano Lett. **4**, 35 (2004).
[37] G. Pennington and N. Goldsman, Phys. Rev. B **68**, 045426 (2003).

Downloaded 18 Oct 2006 to 129.6.121.139. Redistribution subject to AIP license or copyright, see http://jap.aip.org/jap/copyright.jsp